# Size-adapted segmentation of individual mammographic microcalcifications

Nikolaos S. Arikidis, Anna Karahaliou, Spiros Skiadopoulos, Panayiotis Korfiatis, Eleni Likaki, George Panayiotakis and Lena Costaridou

*Abstract*—**Accurate Microcalcification (MC) segmentation is a crucial first step in morphology based Computer Aided Diagnosis systems for microcalcifications in mammography. In this article we present an automated segmentation method of individual MCs adaptive to both size and shape variations. Size is estimated by active rays (polar-transformed active contours) on continuous wavelet representation while shape adaptivity is achieved by a subsequent region growing step. Following MC seed point annotation, contour point estimates are obtained by implementing active rays on an analytic scale-space representation in a coarse-to-fine strategy. Initial coarsest scale is automatically defined by analyzing MC responses across scales. A region growing method is used to delineate the final MC contour curve, with pixel aggregation constrained by the MC contour point estimates. The segmentation accuracy of the proposed method was quantitatively evaluated by means of area overlap by comparing automatically derived borders with manually traced ones provided by an expert radiologist. The proposed method achieved an area overlap of 0.68±0.13 on a dataset of 67 individual microcalcifications, originating from pleomorphic clusters.**

***Index Terms*— active rays, continuous wavelet transform, microcalcification segmentation, region growing, size-adapted scale-space analysis.**

## I. Introduction

Morphology analysis is important for the diagnosis of microcalcifications (MCs), as a means of quantifying size and shape properties of individual microcalcification within a cluster or of the entire microcalcification cluster, according to the BI-RADS lexicon [1]. A number of authors have utilized a wide range of quantitative individual microcalcification morphology and intensity properties [2]-[4]. Accurate MC segmentation has a key-role in Computer aided diagnosis (CAD) systems performance, influencing morphologic feature extraction of individual microcalcifications.

Accurate segmentation of individual microcalcifications remains a difficult task, challenged by microcalcifications size and shape variability, superimposed surrounding tissues and high frequency noise.

Segmentation of individual MCs has been achieved by grey-level based methods with empirically defined parameters such as region growing [5] and grey-level thresholding on pre-processed ROIs [6]-[8]. To fulfill CAD requirements for real-time behavior and parameter-free segmentation, more sophisticated techniques have been proposed such as morphologic operations [9]-[11], watershed algorithms [12], [13], Bayesian pixel classification combined with MRF models [14] and radial gradient based methods [13],[15].

A segmentation method was recently proposed to deal with MC size variability [15]. Specifically, active rays (polar-transformed active contours) were implemented on B-spline wavelet representation to identify microcalcification contour point estimates. Contour points are estimated in a coarse-to-fine strategy initialized however at a fixed dyadic scale.

The current study provides robust scale selection for initializing the coarse-to-fine strategy for MC segmentation, aiming to adapt on a wide range of MC sizes. A continuous wavelet transform (CWT) is used to provide normalized Laplacian multiscale representation where MC scale-space signatures are estimated. MC scale-space signatures are defined as the local maxima of the wavelet transform coefficients both along scale and spatial variables. These variables are subsequently used to initialize the active rays coarse-to-fine implementation across consecutive scales, for estimating MC contour points. MC delineation is achieved by region growing constrained by MC contour points. Segmentation accuracy of the method is evaluated quantitatively by means of area overlap on a dataset of 67 individual MCs.

Manuscript received August 13, 2008. This work was supported in part by the Caratheodory Programme (C.183) of the University of Patras

N. Arikidis is with the Medical Physics Department of University of Patras, Greece ( arikidis@upatras.gr)

A. Karahaliou is with the Medical Physics Department of University of Patras, Greece ( karahaliou.a@med.upatras.gr)

S. Skiadopoulos is with the Medical Physics Department of University Hospital of Patras, Greece ( skiado@med.upatras.gr)

P. Korfiatis is with the Medical Physics Department of University Hospital of Patras, Greece ( korfp@upatras.gr )

E. Likaki is with the Radiology Department of University Hospital of Patras, Greece ( likaki@med.upatras.gr)

G. Panayiotakis is with the Medical Physics Department of University Hospital of Patras, Greece ( panayiot@upatras.gr)

L. Costaridou is with the Medical Physics Department of University of Patras, Greece (phone +302610969111; fax: +30261996113; e-mail: costarid@upatras.gr).

## II. Materials and Methods

### A. Dataset

The case sample consists of 67 individual MCs of varying sizes and shapes, originating from 37 microcalcification clusters. All mammograms were selected from the Digital Database for Screening Mammography (DDSM), digitized with a LUMISYS laser scanner at a pixel depth of 12-bits and a pixel size of 50 μm. Figure 1 illustrates the distribution of the 67 individual MCs analyzed in our dataset, with respect to size (estimated by minimum and maximum length parameter).

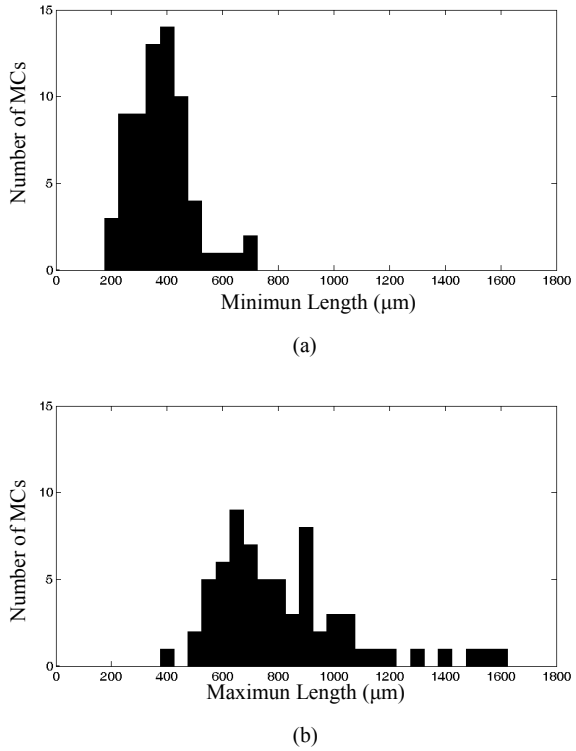


Fig. 1. Histogram depicting the distribution of individual MCs with respect to (a) minimum and (b) maximum length parameter.

### B. Estimating MC scale-space signatures with Continuous Wavelet Transform

MCs cover a small number of image pixels and appear usually as bright or slightly elongated spots in the mammogram. Strickland [16] specifically modelled the average gray level profile of MCs by circularly symmetric Gaussian function. According to matched filter theory [17], the Laplacian of the Gaussian filter maximizes its response at the location of Gaussian like patterns in a noisy image. To reliable detect all potential MCs within an image, local maxima in Laplacian convolved images must be considered on a range of scales. Methods concerning the scale of objects to be detected by using convolutions for different kernel sizes are referred to as scale-space approaches [18]. Netch [17] estimated MC scale-space signatures from local maxima of normalized Laplacian responses across consecutive scales.

CWT is a mathematical tool that inherently can provide a normalized Laplacian representation. CWT provides a scale-space representation by convolving the image with a family of shifting $\alpha$ and scaling $s$ functions

$$h_{s,a}(x) = |s|^{-1} h((x-a)/s) \qquad (s, a \in \Re, s \neq 0) \qquad (1)$$

defined from a single function $h : \Re \to \Re$ is called a wavelet. Provided that $h$ satisfies certain admissibility conditions

$$\int_{\omega=-\infty}^{\infty} \frac{|\hat{h}(\omega)|^2}{|\omega|} d\omega < \infty \qquad (2)$$

then the representation $Wf : \Re\{0\} \times \Re \to \Re$ given by

$$(Wf)(s,a) = \langle f, h_{s,a} \rangle = |s|^{-1} \int_{x \in \Re} f(x) h((x-a)/s) dx \qquad (3)$$

is called the CWT of $f : \Re \to \Re$. The scale-space representation can be considered to be a special case of CWT, where the scale-space axioms imply that the function $h$ must be selected as a derivative of the Guassian kernel. This representation was suggested for image analysis by Mallat [19].

In this study we applied the Mexican Hat wavelet (equivalent to the Laplacian-of-Gaussian function) where the 2d continuous wavelet transform is given by

$$(Wf)(s,a,b) = |s|^{-1} \int_{y \in \Re} \int_{x \in \Re} f(x,y) h\left( \frac{(x-a)}{s}, \frac{(y-b)}{s} \right) dxdy \qquad (4)$$

MC scale-space signatures were defined as the local maxima of the wavelet transform coefficients both along scale and spatial variables.

### C. Size-adapted MC segmentation

Those variables were used to automatically initialize the coarse-to-fine approach of Active Rays segmentation method to estimate the MC contour points. Active rays (polar transformed active contours) reduce the contour points search from the 2D image plane to a 1D signal for an orientation $\theta$, introducing a unique ordering in the image plane and thus reducing computation time [20]. In this work, active rays are implemented in the Laplacian scale-space representation, which inherently incorporates smoothness constraints, providing robustness to noise and spurious edges. MC contour points were estimated at 8 orientations, while scale variable ranged from 1 to 8 by steps of 0.2. The MC contour was

finally delineated with a region growing technique, constrained by the MC boundary estimates [15].

### *D. Evaluation of Segmentation Accuracy*

Quantitative segmentation accuracy assessment has been utilized in mammography either for simulated or real MCs [12], [21]. However, due to difficulty and time required in defining the exact ground truth, qualitative evaluation by means of subjective rating scales is an alternative approach, also recently adopted [13].

In the current study, segmentation accuracy of the proposed method, as well as of the modified version, was quantitatively evaluated by means of the area overlap [12]. An expert radiologist defined the ground truth by generating manual outlines of individual MCs.

The area Overlap between "ground truth" (O) and computer (C) derived borders is defined by:

$$Overlap = \frac{O \cap C}{O \cup C} \tag{5}$$

The value of Overlap is bound between zero (no overlap) and one (exact overlap).

To test if the differences in performance between the two segmentation methods is statistically significant or not, two-tailed Student's t-test for paired data was performed. Derived values of $p<0.05$ indicate statically significant difference.

## III. RESULTS

Figure 2(a) depicts Regions of Interest (ROIs) containing MCs. Figure 2(b) depicts individual MCs segmented by active rays coarse-to-fine implementation across consecutive scales, with automatically selected initial coarse scale, followed by region growing. Delineations provided by an experienced radiologist (ground truth) are depicted in Figure 2(c). As it is observed, the proposed method has efficiently segmented MCs of various sizes and of various shapes.

Figure 3 depicts the automatically selected initial coarse scale used in the coarse–to-fine implementation of active rays segmentation for each of 67 MCs of the dataset. As it is observed, most of the MC scale-space signatures are detected at scales s=3 to s=4.

To demonstrate the efficiency of the automatically selected initial coarse scale, the segmentation was modified by selecting two fixed initial coarse scales (s=3 and s=4) to initialize coarse-to-fine strategy. Figure 4 illustrates area overlap values for the 67 MCs of the dataset, segmented with automatically selected initial coarse scale (white bars) as well as with fixed initial coarse scale s=3 (gray bars) and s=4 (black bars). Corresponding mean and standard deviation values of area overlap are summarized in Table I.

The method with automatically selected initial coarse scale demonstrated a similar segmentation accuracy as compared to s=4 ($p>0.05$), and a statistically significantly higher performance as compared to s=3 ($p<0.05$).

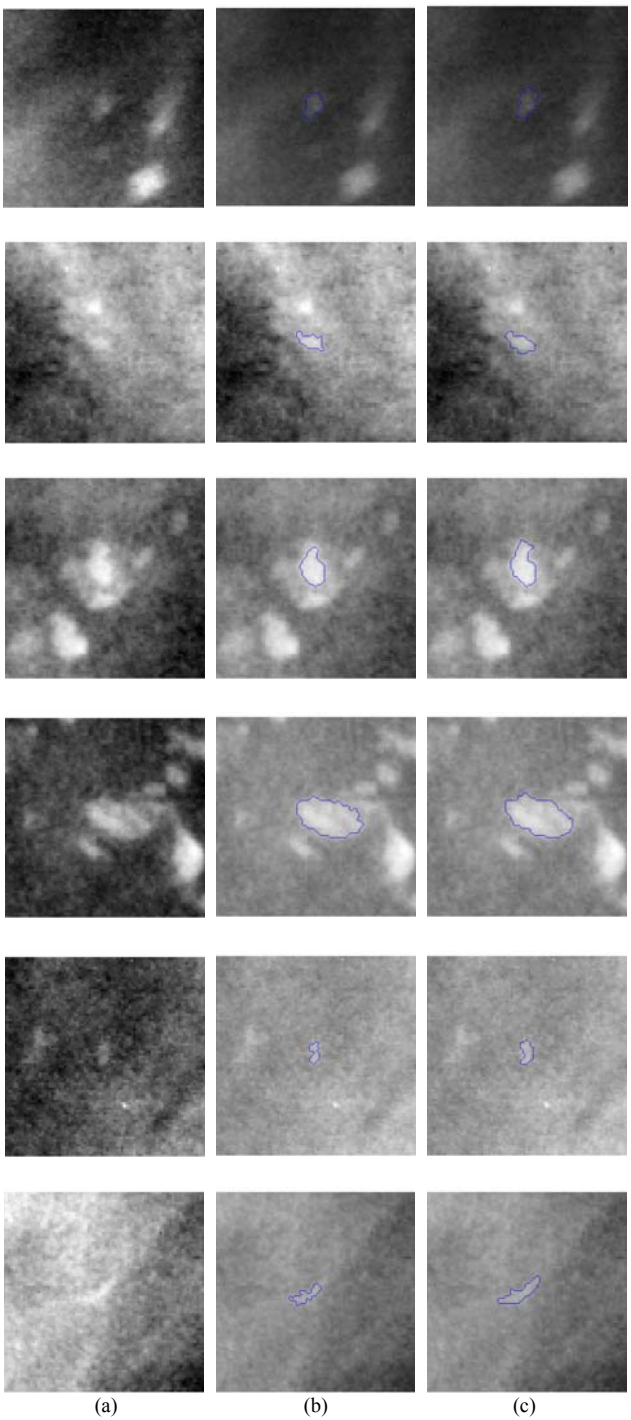


Fig. 2. Segmentation example of 6 individual MCs (a) Original ROIs (81x81 pixels) containing the individual microcalcifications. (b) Segmentations provided by active rays coarse-to-fine implementation across consecutive scales, with automatically selected initial coarse scale, followed by region growing, (c) Segmentations provided by an experienced radiologist (ground truth).

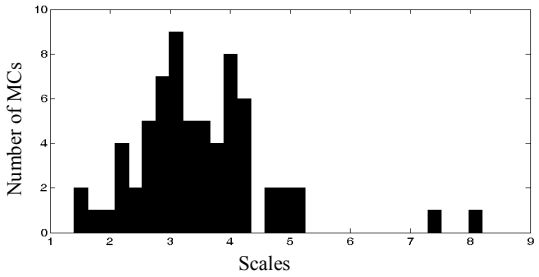


Fig. 3. Automatically selected initial coarse scales used in the coarse-to-fine implementation of active rays segmentation for each of 67 MCs of the dataset.

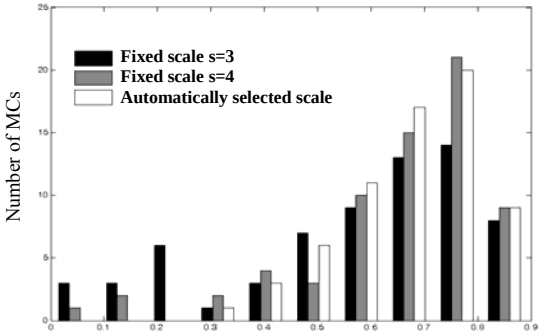


Fig. 4. Area overlap values for the 67 MCs of the dataset, segmented by active rays with automatically selected initial coarse scale (white bars) as well as with fixed initial coarse scale s=3 (black bars) and s=4 (gray bars).

TABLE I
SEGMENTATION ACCURACY OF ACTIVE RAYS COARSE-TO-FINE IMPLEMENTATION WITH COARSE SCALE AUTOMATICALLY DEFINED AND WITH MANUALLY SELECTED COARSE SCALES

| Initial coarse scale | Mean | Standard Deviation |
|---|---|---|
| Automatically defined | 0.68 | 0.13 |
| *Fixed S=3* | 0.57 | 0.23 |
| *Fixed S=4* | 0.65 | 0.18 |

## IV. DISCUSSION

In a previous effort for MC segmentation, active rays were implemented on B-spline wavelet representation to identify MC contour point estimates in a coarse-to-fine strategy at a limited number of scales [15]. MC contour points were subsequently used to constrain a region growing technique.

In the current study the CWT was employed to automatically detect MC scale-space signatures to initialize actives rays coarse-to-fine implementation for MC segmentation. The robust coarse scale selection in combination with the analytic scale-space representation provided by the CWT enhances the performance of the active rays segmentation method by adapting to wide range of MC sizes and avoiding spurious edges.

In the dataset analyzed, most of MC scale-space signatures are detected at scale s=3 and s=4 (Fig. 3). To illustrate the advantages offered by the automatically selected initial coarse scale of active rays segmentation, the method was also implemented with a fixed initial coarse scale s=3 and s=4.

Results of the quantitative segmentation accuracy evaluation suggest that robust coarse scale selection has a better or equal performance as compared to manually defined coarse scale s=3 and s=4 respectively (Fig. 4, Table I). In an unknown dataset, characterized by wide range of MC sizes, manual selection of coarse scale is both impractical (i.e. empirically defined) and suboptimal (i.e. only a specific range of MC sizes will be efficiently segmented).

Difficulty and time required in defining the exact MC ground truth has motivated qualitative evaluation by means of subjective rating scales [13].

While only one study has adopted a similar quantitative segmentation accuracy assessment for real MCs [12], difference in dataset does not allow direct comparison.

Future efforts should consider expansion of the dataset as well as method performance comparison to inter- and intra-observer variability.

## V. CONCLUSION

The current study provides a robust scale selection algorithm for initializing a coarse-to-fine strategy for MC segmentation, aiming to adapt on a wide range of MC sizes. The method exploits CWT properties to detect MC scale-space signatures to initialize actives rays coarse-to-fine implementation for MC segmentation.

Results of the current study suggest that robust coarse scale selection can contribute to MC segmentation by adapting to wide range of MC sizes and avoiding spurious edges.

Morphology based CAD schemes for MCs can take advantage of size adapted MC segmentation methods.

## REFERENCES

[1] M. Muller-Schimpfle, A. Wersebe, T. Xydeas, A. Fischmann, U. Vogel, N. Fersis, C. D. Claussen and K. Siegmann, "Microcalcifications of the breast: How does radiologic classification correlate with histology?" *Acta Radiol.*, vol. 46, no. 8, pp. 774-781, 2005.

[2] A. Papadopoulos, D. I. Fotiadis, and A. Likas, "Characterization of clustered microcalcifications in digitized mammograms using neural networks and support vector machines," *Artif. Intell. Med.*, vol. 34, no. 2, pp. 141-150, 2005.

[3] J. Sklansky, E. Y. Tao, M. Bazargan, C. J. Ornes, R. C. Murchison, and S. Teklehaimanot, "Computer-aided, case-based diagnosis of mammographic regions of interest containing microcalcifications," *Acad. Radiol.*, vol. 7, no. 6, pp. 395-405, 2000.

[4] Y. Jiang, R. M. Nishikawa, R. A. Schmidt, C. E. Metz, M. L. Giger and K. Doi, "Improving Breast Cancer Diagnosis with Computer-aided Diagnosis," *Acad. Radiol.*, vol. 6, no. 1, pp. 22-33, 1999.

[5] H. P. Chan, B. Sahiner, K. L. Lam, N. Petrick, M. A. Helvie, M. M. Goodsitt and D. D. Adler, "Computerized analysis of mammographic microcalcifications in morphological and texture feature spaces," *Med. Phys.*, vol. 25, no. 10, pp. 2007-2019, 1998.

[6] I. Leichter, R. Lederman, S. Buchbinder, P. Bamberger, B. Novak and S. Fields, "Optimizing Parameters for Computer-aided Diagnosis of Microcalcifications at Mammography," *Acad. Radiol.*, vol. 7, no. 6, pp. 406-412, 2000.

[7] S. S. Buchbinder, I. S. Leichter, R. B. Lederman, B. Novak, P. N. Bamberger, H. Coopersmith and S. I. Fields, "Can the Size of Microcalcifications Predict Malignancy of Clusters at Mammography?" *Acad. Radiol.*, vol. 9, no. 28, pp. 18-25, 2002.

[8] M. Kallergi, "Computed-aided diagnosis of mammographic microcalcification clusters," *Med. Phys.*, vol. 31, no. 2, pp. 314-326, 2004.

[9] O. Tsujii, M. T. Freedman, and S. K. Mun, "Classification of microcalcifications in digital mammograms using trend-oriented radial basis function neural network," *Pattern Recognit.*, vol. 32, no. 5, pp. 891-903, 1999.

[10] H. Soltanian-Zadeh, F. Rafiee-Rad, and S. D. Pourabdollah-Nejad, "Comparison of multiwavelet, wavelet, Haralick, and shape features for microcalcification classification in mammograms," *Pattern Recognit.*, vol. 37, no. 10, pp. 1973-1986, 2004.

[11] J. C. Fu, S. K. Lee, S. T. C. Wong, J. Y. Yeh, A.H. Wang and H .K. Wu, "Image segmentation feature selection and pattern classification for mammographic microcalcifications," *Comput. Med. Imaging Graph.*, vol. 29, no. 6, pp. 419-429, 2005.

[12] D. Betal, N. Roberts, and G. H. Whitehouse, "Segmentation and numerical analyis of microcalcifications on mammograms using mathematical morphology," *Br. J. Radiol.*, vol. 70, no. 837, pp. 903-917, 1997.

[13] S. Paquerault, L. M. Yarusso, J. Papaioannou, Y. Jiang and R. M. Nishikawa, "Radial gradient-based segmentation of mammographic microcalcifications: Observer evaluation and effect on CAD performance," *Med. Phys.*, vol. 31, no. 9, pp. 2648-2657, 2004.

[14] W. J. H. Veldkamp, N. Karssemeijer, J. D. M. Otten, and J. H. C. L. Hendrinks, "Automated classification of clustered microcalcifications into malignant and benign types," *Med. Phys.*, vol. 27, no. 11, pp. 2600–2608, 2000.

[15] N. Arikidis, S. Skiadopoulos, A. Karahaliou, E. Likaki, G. Panayiotakis and L. Costaridou, "Integrating multiscale active contours and region growing for microcalcifications segmentation in mammography," *Nucl. Instrum. Methods Phys. Res. A*, to be published.

[16] R. N. Strickland and H. I. Hahn, "Wavelet transforms for detecting microcalcifications in mammograms," *IEEE Trans. Med. Imaging,* vol. 15, no. 2, pp. 218–228, Apr. 1996.

[17] T. Netsch and H. O. Peitgen, "Scale-space signatures for the detection of clustered microcalcifications in digital mammograms," *IEEE Trans. Med. Imaging*, vol. 18, no. 9, pp. 774-786, Sep. 1999.

[18] T. Lindeberg, *Scale-Space Theory in Computer Vision*, Boston: Kluwer Academic Publishers, 1997.

[19] S. Mallat and S. Zhong, "Characterization of signals from multiscale edges," *IEEE Trans. Pattern Anal. Mach. Intell.*, vol. 14, no. 7, pp, 710–732, July 1992.

[20] J. Denzler and H. Niemann, "Active rays: polar-transformed active contours for real-time contour tracking," Real-Time Imaging, vol. 5, no. 3, pp. 203-213, 1999.

[21] W. J. Veldkmp and N. Karssemeijer, "Accurate segmentation and contrast measurement of microcalcifications in mammograms: A phantom study," *Med. Phys.*, vol. 25, no. 7, 1998.